

Article

# Black TiO<sub>2</sub> Thin Films Production Using Hollow Cathode Hydrogen Plasma Treatment: Synthesis, Material Characteristics and Photocatalytic Activity

Armstrong Godoy Junior <sup>1,\*</sup>, André Pereira <sup>2</sup>, Marcilene Gomes <sup>3</sup>, Mariana Fraga <sup>4</sup>, Rodrigo Pessoa <sup>1</sup>, Douglas Leite <sup>1</sup>, Gilberto Petraconi <sup>1</sup>, Adailton Nogueira <sup>5</sup>, Heberton Wender <sup>5</sup>, Walter Miyakawa <sup>6</sup>, Marcos Massi <sup>7</sup> and Argemiro da Silva Sobrinho <sup>1,\*</sup>

<sup>1</sup> Laboratório de Plasmas e Processos (LPP), Instituto Tecnológico de Aeronáutica (ITA), São José dos Campos, SP 12228-900, Brazil; rspessoa@ita.br (R.P.); leite@ita.br (D.L.); petra@ita.br (G.P.)

<sup>2</sup> Grupo de Pesquisa em Materiais Fotônicos e Energias Renováveis (MaFER), Universidade Federal de Grande Dourados (UFGD), Dourados, MS 79825-070, Brazil; andreljpereira@gmail.com

<sup>3</sup> Instituto Federal de Educação, Ciência e Tecnologia de São Paulo (IFSP), São José dos Campos, SP 12223-201, Brazil; marcilenegomes@gmail.com

<sup>4</sup> Instituto de Ciência e Tecnologia (ICT), Universidade Federal de São Paulo (Unifesp), São José dos Campos, SP 12231-280, Brazil; mafraga@ieee.org

<sup>5</sup> Laboratory of Nanomaterials and Applied Nanotechnology, Institute of Physics, Federal University of Mato Grosso do Sul, Av. Costa e Silva S/N, Bairro Universitário, Campo Grande, MS 79070-900, Brazil; adailtonchimenes@gmail.com (A.N.); heberton.wender@ufms.br (H.W.)

<sup>6</sup> Instituto de Estudos Avançados (IEAv), São José dos Campos, SP 12228-001, Brazil; walter.toshi@gmail.com

<sup>7</sup> Universidade Presbiteriana Mackenzie, São Paulo, SP 01302-907, Brazil; marcos.massi@mackenzie.br

\* Correspondence: godoyajr@gmail.com (A.G.J.); argemiro@ita.br (A.d.S.S.)

Received: 12 January 2020; Accepted: 19 February 2020; Published: 2 March 2020



**Abstract:** Black TiO<sub>2</sub> materials have been quite widely explored due to their large solar absorption and superior photocatalytic activity. In this paper, the blackening process of titanium dioxide (TiO<sub>2</sub>) thin film using the hollow cathode hydrogen plasma (HCHP) technique is reported. First, pristine anatase TiO<sub>2</sub> films were grown by magnetron sputtering onto silicon and cover glass substrates and then annealed at 450 °C for 2 h. Then, the as-grown TiO<sub>2</sub> films were treated with HCHP for 15 min. The physical, chemical and morphological properties of the films were analyzed by profilometry, X-ray diffraction (XRD), UV-Vis spectrophotometry, Raman spectroscopy, X-ray photoelectron spectroscopy (XPS) and atomic force microscopy (AFM) techniques. Electrical and photocatalytic measurements were performed by four-point probe and methylene blue UV degradation assays, respectively. The results showed that the black TiO<sub>2</sub> film is highly absorbent in the UV-visible region, has low electrical resistance and greater surface area compared to the non-treated TiO<sub>2</sub> film. These properties of black TiO<sub>2</sub> film, as well as its performance as a photocatalytic agent, were investigated, indicating the superior quality of this material in thin film form and the promising potential of the HCHP treatment to produce hydrogenated TiO<sub>2</sub> in short process time.

**Keywords:** black titanium dioxide; magnetron sputtering; hollow cathode; hydrogen plasma; photocatalysis

## 1. Introduction

Over the centuries, due to the unreasonable use of the planet's resources and the reduction of water resources, the increased need for renewable energy sources and food production are currently considered as urgent problems to be solved, facts that have motivated countless studies focused on the

synthesis and modification of materials with direct application to mitigate these problems [1–3]. In the matter of water resources, since the discovery of photocatalytic effect on water splitting by Fujishima and Honda in the early 1970s, photocatalytic processes using semiconductor materials have been seen as a promising method for decomposing liquid contaminants due to their major benefits: low cost, environmental friendliness, and sustainability [4].

Among the most studied photocatalytic materials, titanium dioxide ( $\text{TiO}_2$ ) has been outstanding due to characteristics such as availability, nontoxicity, high chemical inertness, photo corrosion resistance, long-term stability, and commercial inexpensiveness [5]. On the other hand,  $\text{TiO}_2$  has a wide bandgap on the order of 3.2 eV, which limits its photocatalytic activity only to the narrow light-response range of the ultraviolet (UV), i.e., only a small amount of solar radiation reaching the Earth's surface is harnessed [6]. Several approaches, such as the incorporation of metallic or non-metallic dopants into  $\text{TiO}_2$ -based materials, have been explored to increase the absorption rate of this material as much as possible in the entire range of the solar spectrum [7–9]. However, this approach is still a matter of much discussion, as dopants can attract holes, thus behaving as recombination centers that affect the efficiency of photoinduced processes [10]. Additionally, heterojunctions by coupling two semiconductors are also a method that has been studied to improve the photocatalytic activities [11,12]. Alternatively, early in the last decade, the hydrogenation treatment of  $\text{TiO}_2$  triggered intense research interest. The hydrogenated  $\text{TiO}_2$ , which usually has a gray or black color, exhibits significant optical absorption in the UV-infrared spectrum region [13]. Chen and co-workers were the first to demonstrate the hydrogenated or “black”  $\text{TiO}_2$  nanoparticles with a narrow bandgap ( $\approx 1.54$  eV) [13]. Nevertheless, for black titania synthesis, extreme process conditions were required, such as hydrogen gas ( $\text{H}_2$ ) pressures of about tens bar and annealing times of days, which makes this process unfeasible.

Since then, different alternative proposals for black  $\text{TiO}_2$  synthesis have been studied, such as low- or high-pressure heat treatment using different gases [14,15], laser-based processes [16], and plasma-assisted treatment [17], among others [18,19]. All of these proposals focus on reducing the working pressure or using other gases combined with hydrogen to reduce the hazardousness of the process using pure  $\text{H}_2$  under high pressure.

Recently, low-pressure plasma-assisted processes have been used in the hydrogenation of  $\text{TiO}_2$  nanostructures and thin films [20,21]. When the process is performed at reduced pressure, there is no problem using  $\text{H}_2$  gas, and the possibility of contamination of the final material is significantly reduced. Wang et al. prepared black  $\text{TiO}_2$  nanostructures and films in a thermal plasma furnace by 200 W  $\text{H}_2$  plasma for 4–8 h at 500 °C. They performed photodegradation assays with methyl orange under sunlight, verifying a complete degradation after 5 min for black  $\text{TiO}_2$  nanoparticles versus 12 min for pristine  $\text{TiO}_2$  [22]. Wu et al. demonstrated a 40 W  $\text{H}_2$  PECVD treatment for 1.5 h to improve the electrochemical properties of anatase titania nanotube arrays for potential application in supercapacitors [20]. Additionally, Yan et al. reported on the fast lithium storage performance of hydrogenated commercial anatase  $\text{TiO}_2$  nanoparticles prepared by a 3000 W inductively coupled plasma (ICP) hydrogen plasma treatment at 390 °C for 3 h [21]. In another study, Yan et al. synthesized H- $\text{TiO}_2$  nanoparticles with different hydrogenation degrees through 3000 W ICP-CVD hydrogen plasma treatment at 150 °C [23]. The hydrogenation degree was controlled by varying treatment time from 0.5 to 20 min. They investigated the photodegradation of methylene blue (MB) and found that the 0.5 min sample showed better efficiency in its reduction. Panomsuwan et al. synthesized black titania nanoparticles via atmospheric pressure water-plasma technique [24]. They performed photocatalysis under visible-light irradiation and verified the almost total degradation of the MB dye after 180 min using the black  $\text{TiO}_2$  nanoparticles, against the imperceptible degradation when they used the non-hydrogenated  $\text{TiO}_2$  nanoparticles as photocatalytic material under the same process conditions. Mohammadzadeh et al. produced thin layers of anatase titanium dioxide, which coated the glass by the spray pyrolysis method [25]. The layers were hydrogenated by DC plasma from room temperature to 350 °C. They verified the maximum MB degradation (20%) for the 200 °C sample. In a recent study, Islam et al. presented a methodology to produce black  $\text{TiO}_2$  thin films: first,  $\text{TiO}_2$  thin

films were prepared by a surfactant templated sol-gel method and, subsequently, treated with 400 W microwave-assisted CVD hydrogen plasma for 30 min [26]. They performed photoelectrochemical water oxidation measurements that evidenced an increase in the photocurrent of ca. 28 times under UV light and 8 times under blue light.

Please note that most of the aforementioned studies focus on plasma hydrogenation of TiO<sub>2</sub> nanoparticles; only a few studies have investigated black titania in the form of thin film. As is known, TiO<sub>2</sub> in a nano powder form is conducive to surface reactions due to its large active surface area. However, the difficulty in precipitating and recovering the nano powder from the treated liquid limits its application [27]. Therefore, the use of thin films in contaminated liquid photocatalytic processes is interesting and convenient.

The main characteristics that are relevant after the TiO<sub>2</sub> hydrogenation process are: (i) the engineered-disorder-surface; (ii) the existence of Ti<sup>3+</sup> species, oxygen vacancy states and surface hydroxyl (OH) groups; (iii) bandgap narrowing; and (iv) valence band edge [28]. Due to their motivating characteristics, black TiO<sub>2</sub> materials have been widely used in many areas, among which we can highlight the photocatalysis processes [29], hydrogen generation [30], solar desalination [31], dye-sensitized solar cells [32], supercapacitors [33], and photothermal therapy [34].

As an alternative to expensive high-density plasma sources such as ICP and electron cyclotron resonance (ECR) plasma, hollow cathode-based plasmas have arisen [35,36]. These plasmas are attractive due to a simple modification of the biased electrode (cathode), from the usual plane geometry to a hollow configuration which significantly enhances the ionization efficiency of the gas discharge at lower pressures. This occurs because of electrostatic trapping of electrons in the discharge volume called hollow cathode effect (HCE), which promotes a drastic increase in ionization and dissociation processes [35–38]. Various applications such as thin film deposition [35], material etching [36], and activation of surfaces [35] have benefited from this plasma technology. Thus, the hollow cathode hydrogen plasma (HCHP) may be interesting for blackening TiO<sub>2</sub> material process due to its potential in generate highly reactive H<sub>2</sub> plasmas and the lack of studies in the literature using this type of plasma source. Indeed, the HCE enhances the generation of hydrogen radicals and ions and, for samples placed on biased electrode, it increases the efficiency of hydrogen incorporation in the lattice material, in addition to modifying the surface morphology due to the incidence of high-energy hydrogen ions. All reactivity of HCHP allows for short treatment times and because of the good plasma uniformity throughout the treatment region, allows not only the blackening of nano powders but also thin films.

In this paper, the blackening process of TiO<sub>2</sub> thin film using the HCHP technique, its material characteristics, and its photocatalytic activity are reported. Before and after the HCHP treatment, the physical, chemical, and morphological properties of the films were measured by profilometry, XRD, UV-Vis spectrophotometry, Raman spectroscopy, XPS, and AFM techniques. In addition, electrical and photocatalytic measurements were performed by four-point probe and methylene blue-dye degradation assays, respectively.

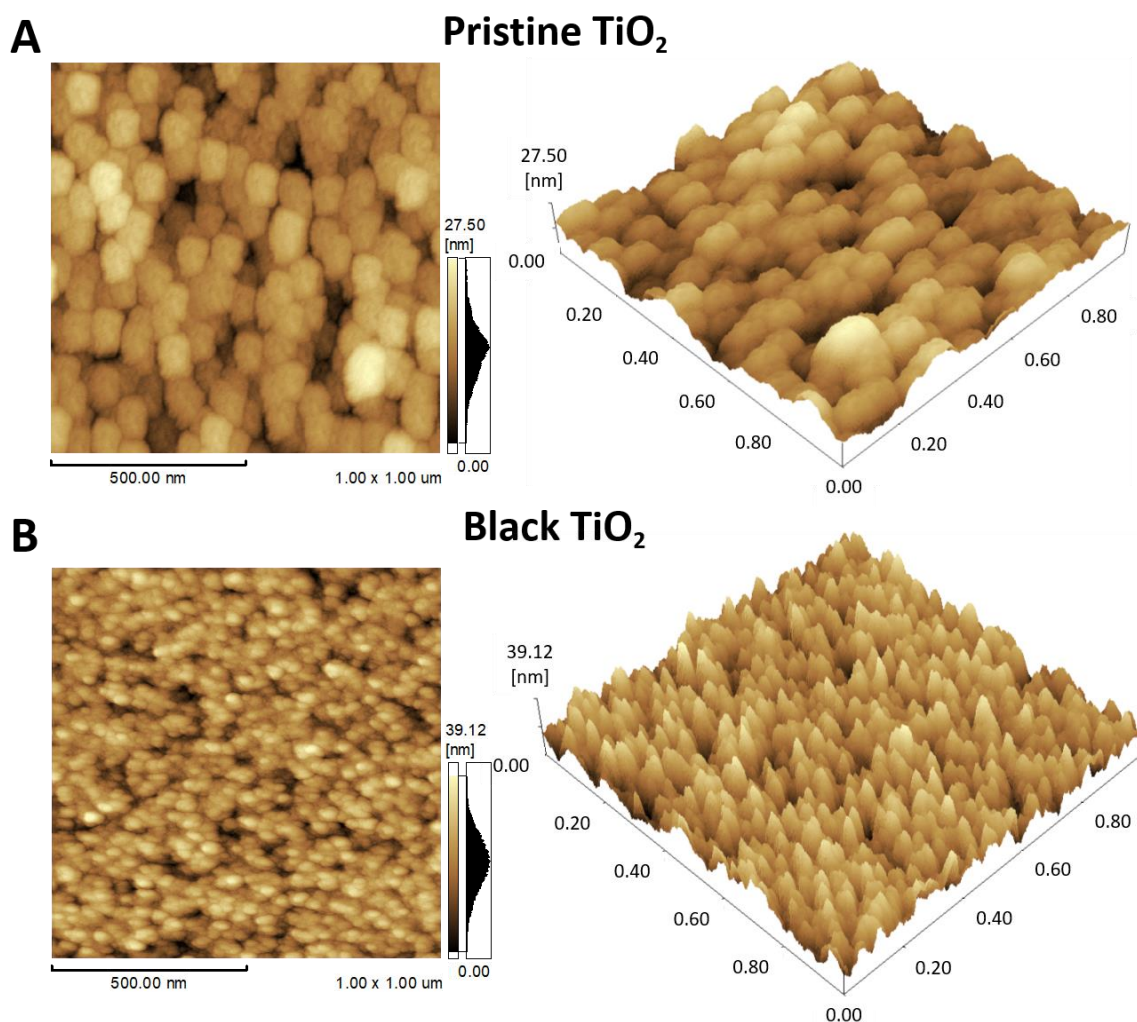
## 2. Results and Discussion

In this section, synthesized TiO<sub>2</sub> thin films are referred to as “Pristine TiO<sub>2</sub>” for pure TiO<sub>2</sub> material and “Black TiO<sub>2</sub>” for HCHP treated pristine TiO<sub>2</sub>. For other details of the samples studied in this work, see Section 3.

### 2.1. Morphological Properties

Figure 1 shows the atomic force microscopy (AFM) images of the pristine and black TiO<sub>2</sub> films. In Figure 1a it can be observed that the surface of the pristine TiO<sub>2</sub> is composed of overlapping 100 nm round particles. For the case of the black TiO<sub>2</sub> surface, Figure 1b shows that it is made up of densely packed agglomerates of particles ranging in size from 40 to 50 nm. Whereas the surface area is a requirement for photocatalytic applications, Table 1 presents the surface area of the pristine and black TiO<sub>2</sub> thin films. Additionally, it presents the values of film thickness and sheet resistance. The black

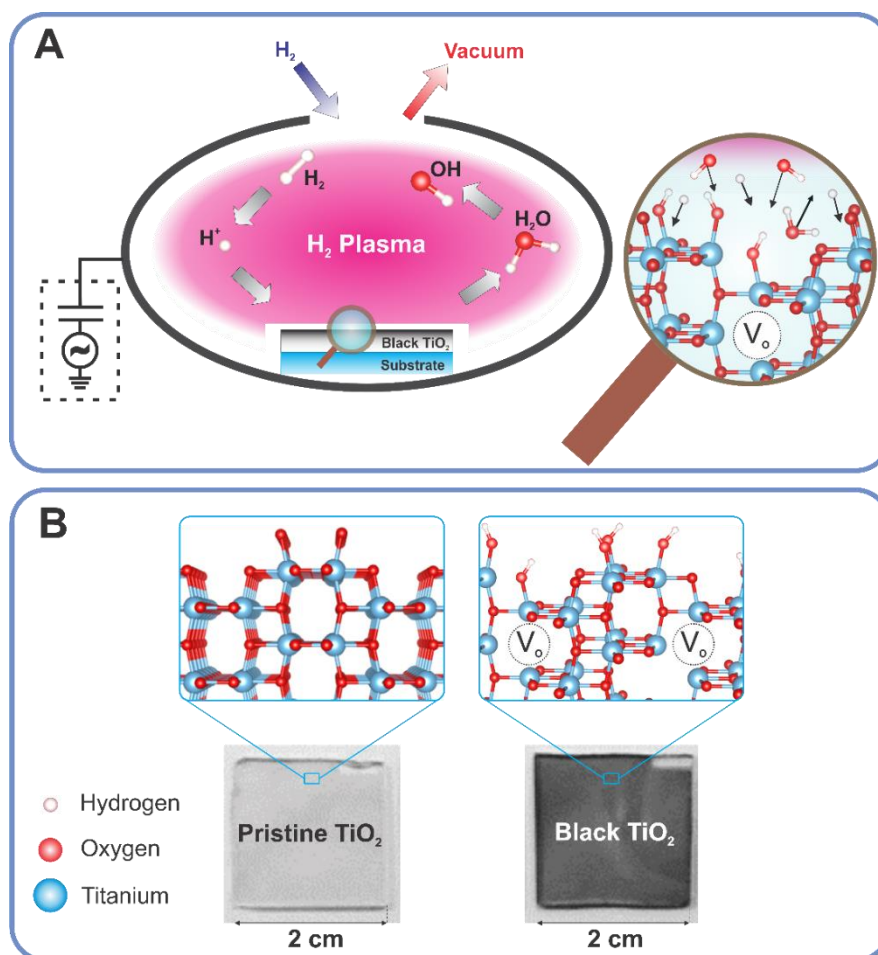
TiO<sub>2</sub> sample has a greater surface area than the pristine one, with an increase of around 24%. This result may be a consequence of the etching effect of hydrogen radicals and ions impinging from the plasma to the TiO<sub>2</sub> surface [39,40]. The H<sub>2</sub> etching of TiO<sub>2</sub> may have caused a preferential ordering of the morphological aspect described above, which favors the increase of the surface area. In addition, the HCHP treatment is found to be responsible for the slight decrease in the thickness of the black TiO<sub>2</sub> thin film. This is an interesting result and probably occurred due to the bombardment of high energy hydrogen ions on the film surface, which can cause a chemical etching of the film surface by generation of volatile species such as OH (see Figure 2a). Also, due to the high energy gained by hydrogen ions when passing through the cathodic plasma sheath (higher than 200 eV [35,36]), some ions can be implanted at depths of several nm, promoting the disordering by formation of oxygen vacancies (V<sub>o</sub>) (see Figure 2b). The combination of these two phenomena could be responsible for the slight thickness decrease, verified by the profilometry analysis. All of these phenomena will be better discussed by XPS analyses in the next section. In addition, further study on HCHP etching of TiO<sub>2</sub> film will be the subject of future work.



**Figure 1.** Topographic and 3D AFM images of (A) pristine and (B) black TiO<sub>2</sub> films.

**Table 1.** Thickness, surface area, lattice parameters, and sheet resistance of the pristine and black TiO<sub>2</sub> thin films.

Sample	Thickness (nm)	Surface Area (μm <sup>2</sup> )	kΩ/sq
Pristine TiO <sub>2</sub>	550 ± 50	1.03	>10 <sup>3</sup>
Black TiO <sub>2</sub>	460 ± 50	1.28	1.93 ± 0.05

**Figure 2.** (A) Schematic diagram of the HCHP detailing the interaction of the hydrogen plasma with the TiO<sub>2</sub> thin film during the blackening process, and (B) Photographs of the produced pristine and black TiO<sub>2</sub> thin films with its respective representative microstructures.

## 2.2. Structural and Chemical Properties

XRD measurements were performed to investigate the microstructural changes that occurred after HCHP treatment. Figure 3 presents the XRD diffractograms of the pristine and black TiO<sub>2</sub> samples. As can be seen, only peaks related to the phase of the tetragonal anatase (ICOD 01-086-1157) are observed for both films. When comparing the films before and after HCHP, it is not possible to observe any significant variation in the diffractograms. This result may be related to the fact that the hydrogenation process may be occurring only on the surface of the films. As the penetration depth of Cu-Kα's X-rays is ~15 microns and the film thickness is ~0.5 microns, the details of the surface cannot be quantified. For this reason, we used Raman scattering measurements to assess the influence of HCHP on the structural properties of the TiO<sub>2</sub> film (see Figure 4).

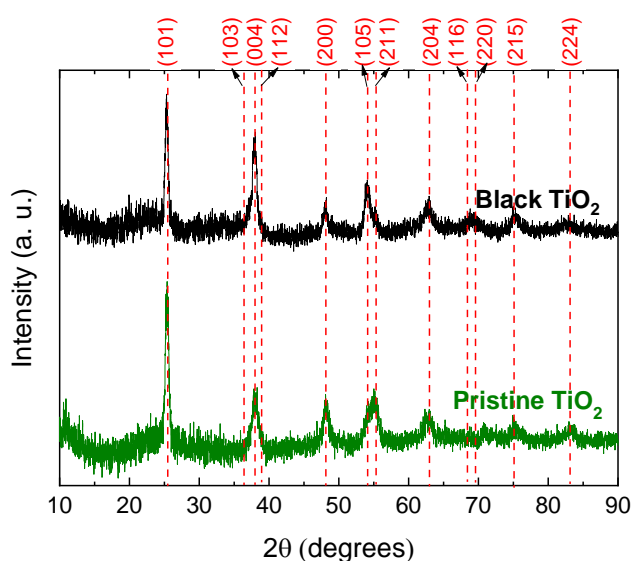


**Figure 3.** XRD diffractograms of pristine and black TiO<sub>2</sub> thin films. The anatase characteristic peaks are highlighted.

Five vibrational modes for both pristine and black TiO<sub>2</sub> films can be observed: E<sub>g</sub> (located around 139.5 cm<sup>-1</sup>, 199.0 cm<sup>-1</sup>, and 632.6 cm<sup>-1</sup>), B<sub>1g</sub> (~390.5 cm<sup>-1</sup>), and A<sub>1g</sub>/B<sub>1g</sub> (~513.3 cm<sup>-1</sup>) (see Figure 4a). These vibration modes are relative to the anatase phase [41,42], corroborating the x-ray diffraction results. Moreover, the heating of the sample during the HCHP process, which reached the temperature of about 260 °C, was not sufficient to initiate the formation of the rutile phase. Hereupon, after the HCHP process a blue-shift and broadening of the most intense E<sub>g</sub> peak were observed (see Figure 4b). These modifications were previously deemed to be a consequence of the creation of oxygen vacancies (V<sub>o</sub>) in the TiO<sub>2</sub> lattice, which indicates an increase in disorder in the black TiO<sub>2</sub> structure compared with the original arrangement of the pristine TiO<sub>2</sub> [13].

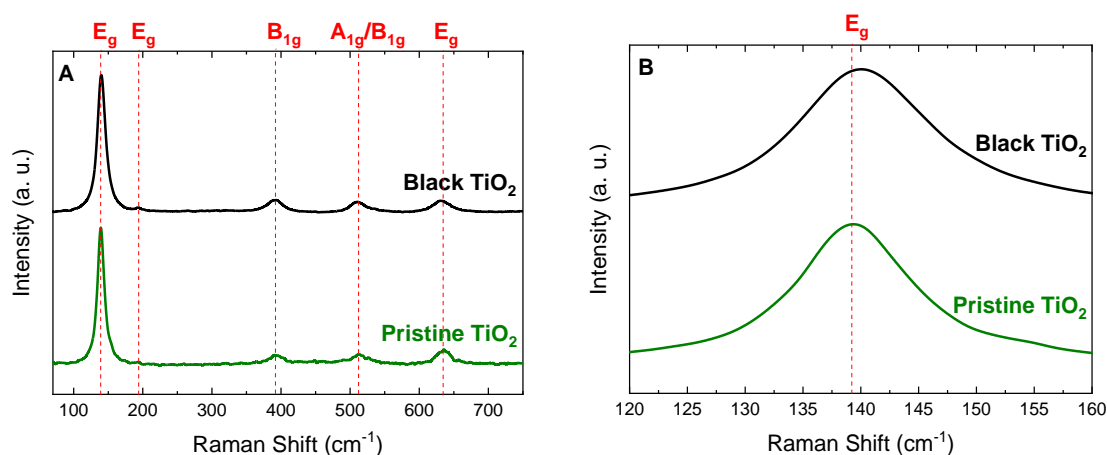


**Figure 4.** (A) Raman spectra of the pristine and black TiO<sub>2</sub> samples, and (B) a focus on the main anatase E<sub>g</sub> vibrational mode.

To investigate the chemical composition of the surface of the samples, XPS measurements were performed. Figure 5 illustrates the Ti 2p<sub>3/2</sub> spectra for both pristine and black TiO<sub>2</sub> samples. The binding energy (BE) and percentage of integrated areas (%area) related to each species are summarized in Table 2. First, it is important to point out that metallic Ti was not noticed in either pristine or black TiO<sub>2</sub> films. As can be observed in Figure 5a, the spectrum was deconvoluted only in one curve located around 459.67 eV, which is assigned to Ti<sup>4+</sup> species [43]. After HCHP treatment, the same spectrum

presented a redshift ( $\sim 0.7$  eV) and now it can be deconvoluted in three curves, attributed mainly to the  $\text{Ti}^{4+}$ ,  $\text{Ti}^{3+}$ , and  $\text{Ti}^{2+}$  species (see Figure 5b) [44]. As shown in Table 2, the black  $\text{TiO}_2$  sample now shows an increase of  $\text{Ti}^{3+}$  and  $\text{Ti}^{2+}$  species, while the concentration of  $\text{Ti}^{4+}$  species decreases. This was probably caused by the creation of oxygen vacancies after the treatment with HCHP [13,44].

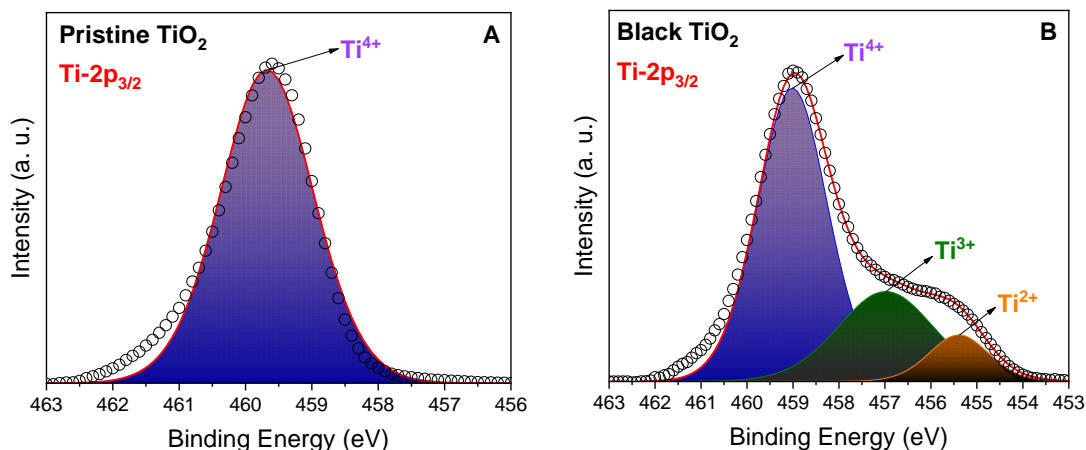


**Figure 5.** High-resolution XPS spectra of  $\text{Ti-2p}_{3/2}$  peaks of the (A) pristine and (B) black  $\text{TiO}_2$  thin films. Open circles and lines represent the experimental and the fitted data, respectively.

**Table 2.** Binding energy (BE) and percentage of integrated area (%area) of the high-resolution  $\text{Ti-2p}_{3/2}$  and  $\text{O1s}$  XPS spectra of pristine and black  $\text{TiO}_2$  samples.

Peaks	Pristine $\text{TiO}_2$		Black $\text{TiO}_2$	
	BE (eV)	%area	BE (eV)	%area
$\text{Ti}^{4+} 2\text{p}_{3/2}$	459.67	100	459.01	64.44
$\text{Ti}^{3+} 2\text{p}_{3/2}$	-	-	456.98	26.89
$\text{Ti}^{2+} 2\text{p}_{3/2}$	-	-	455.39	8.67
$\text{O-H/TiO}_x$	532.12	47.19	531.89	54.17
$\text{Ti-O}$	530.80	52.80	530.59	45.82

Figure 6 presents the  $\text{O1s}$  XPS spectra for the pristine and hydrogenated  $\text{TiO}_2$  samples. Additionally, the respective BE centers are shown in Table 2. The spectra of both films can be deconvoluted into two curves: one centered on  $\sim 530.80$  eV, which is related mainly to  $\text{O}^{2-}$  anion in  $\text{TiO}_2$  [45], and other on  $\sim 532.12$  eV, which is related to hydroxyl groups [46] or  $\text{V}_o$  in titanium oxide ( $\text{TiO}_x$ ) [47]. For the pristine  $\text{TiO}_2$  sample, both options are possible. However, once the heat treatment after the pristine  $\text{TiO}_2$  film deposition at  $450^\circ\text{C}$  was carried out at atmospheric pressure, the  $\text{V}_o$  production was not significant [44], leading us to believe that this peak is mainly related to OH species adsorbed on the film surface. After the HCHP process, a decrease of 7% in the %area for the  $\text{Ti-O}$  curve and an increase of 7% for the  $\text{OH/TiO}_x$  curve was observed (see Table 2). Additionally, the increase in the %area of the curve at 532.12 eV after the HCHP process can be attributed to the generation of  $\text{TiO}_x$  defects.

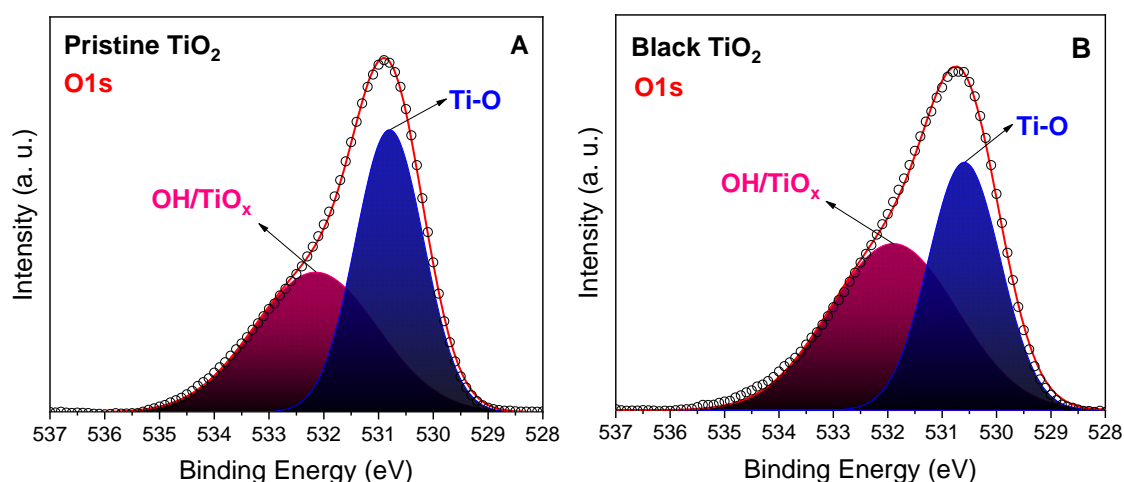
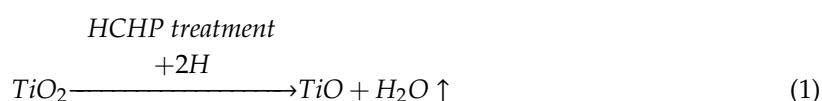


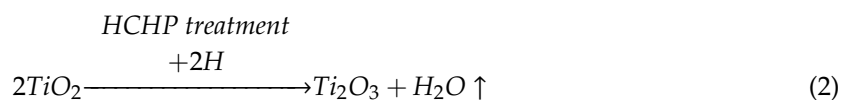
**Figure 6.** High-resolution XPS spectra of O1s peaks of the (A) pristine and (B) black TiO<sub>2</sub> thin films. Open circles and lines represent the experimental and the fitted data, respectively.

It can be noted from the XPS results that, after HCHP treatment, the %area of the OH/TiO<sub>x</sub> peak increases by 7%, while the concentration of Ti<sup>3+/2+</sup> species increases by 35.56%. This fact indicates the possible formation of volatile molecules of H<sub>2</sub>O from the interaction of H<sup>+</sup> ions (coming from the hydrogen plasma) with the surface of the film (see Figure 2a and Equations (1), (2)). These reactions are responsible for the desorption of O atoms from the film surface after HCHP treatment creating V<sub>o</sub> [44]. A more detailed plasma study must be performed in future works to try to better explain the interactions between the H<sub>2</sub> plasma and the TiO<sub>2</sub> film surface.

Another point to be discussed is that a relevant content of Ti<sup>2+</sup> species (8.67%) was observed in the black TiO<sub>2</sub> thin film. Hannula et al. reported that this species is only noticed when the material is exposed to two conditions: (i) heat treatment above 400 °C in an ultra-vacuum reactor or (ii) 5 min at 300 °C under hydrogen atmosphere [44]. Since in this work the sample temperature did not exceed 260 °C, this behavior may be associated with the high energy transferred to the sample during the HCHP treatment, which favored a direct reduction of Ti<sup>4+</sup> to Ti<sup>2+</sup>. Thus, the process of Ti reduction caused by HCHP treatment can be summarized according to the following chemical reactions presented in Equations (1) and (2).



and/or



### 2.3. Optical and Electrical Properties

The thin film blackening is already indicative that, after the HCHP treatment, the black TiO<sub>2</sub> begins to absorb in the visible range (see Figure 2b). As the photoinduced catalytic processes using pure TiO<sub>2</sub> materials are efficient only in the UV range, increasing light absorption in the visible range is also advantageous in photocatalytic applications.

To investigate the influence of the HCHP process on the optical characteristics of the films produced, we carried out UV-vis transmittance measurements as illustrated in Figure 7a. The results show that the pristine TiO<sub>2</sub> thin film is transparent in the visible light spectrum and absorbs light merely below 400 nm, in other words, predominantly in the UV region. The maximums of the transmittance interference fringe (caused by the multiple reflections in the interior of the film) reach the same values as the pure substrate, which is also transparent, with ~90% of transmittance in this spectrum. The missing

10% is due to the reflection (specular + diffuse). In contrast, the black TiO<sub>2</sub> film displays a significant absorption in the visible and NIR regions, in addition to the same absorption in the UV range.

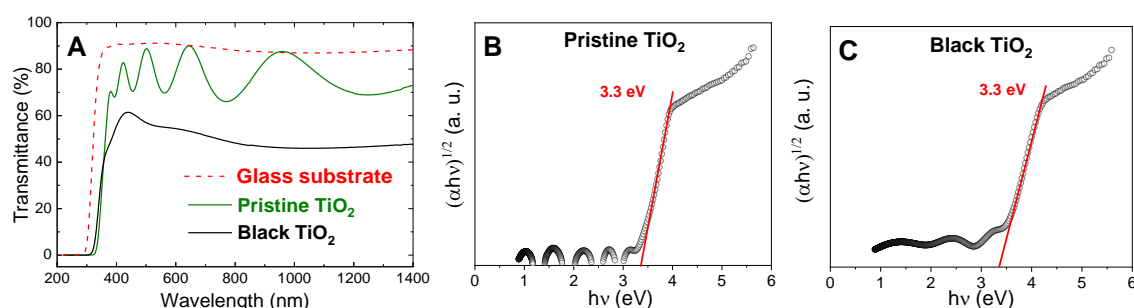


**Figure 7.** (A) UV-vis-NIR transmittance spectra of glass substrate and investigated films; (B,C) Tauc plot curves of the pristine and black TiO<sub>2</sub> films.

Figure 7b,c shows the Tauc plots for pristine and black TiO<sub>2</sub> films, respectively. The bandgap value of both samples is approx. 3.3 eV, which is an indicative that the HCHP process does not produce the expected bandgap narrowing. Therefore, the increase in absorption can be attributed to the creation of Ti<sup>3+/2+</sup> defects [48,49], responsible for an n-type energy level between the valence (VB) and conduction (CB) bands of hydrogenated TiO<sub>2</sub> films (see diagram in Figure 8a) [50]. Additionally, the formation of V<sub>o</sub> is known to increase the TiO<sub>2</sub> disorder, which can increase/create tail states (TS) at the edges of the VB [13], as depicted in Figure 8a.

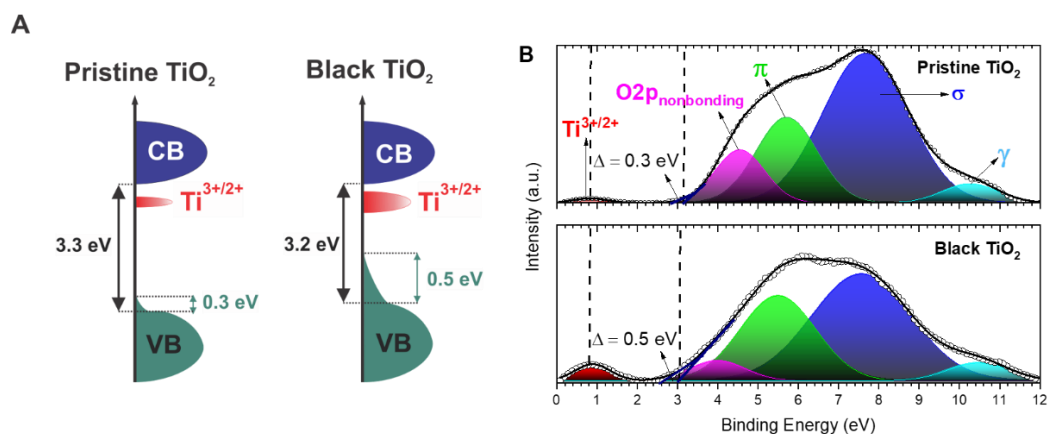


**Figure 8.** (A) Representative diagram of the bandgap details and (B) XPS valence band spectra highlighting the five energy states deconvoluted of the pristine and black TiO<sub>2</sub> thin films.

XPS analysis for low energies was carried out, whose spectra are illustrated in Figure 8b. These spectra are proportional to the occupied density of state (DOS) at the top of the VB and were used to study the electronic properties of the samples produced. First, the value acquired after extrapolate to zero the linear range of the lower energy part at the top of the VB (Figure 8b) is ~3.3 eV for pristine TiO<sub>2</sub> and ~3.2 eV for hydrogenated TiO<sub>2</sub>, indicating that the intrinsic value of black TiO<sub>2</sub> bandgap decreased only slightly with the HCHP process. Given the intrinsic uncertainty of this measurement method (~0.1 eV), this result reinforces the bandgap values inferred by the Tauc plot method (Figure 7b). Additionally, this analysis allows an approximate measurement of the increase in TS size induced by V<sub>o</sub> [13]. Although the pristine TiO<sub>2</sub> not being submitted to the HCHP process, this sample has a TS size ( $\Delta$ ) of ~0.3 eV (see Figure 8b). The inherent defects in films grown by sputtering techniques, such as lattice defects, residual stress and grain contour, may be responsible for the presence of TS in the pristine film [51]. After the HCHP process, the hydrogenated TiO<sub>2</sub> film showed an increase of ~0.2 eV

in its TS size. This increase can be attributed to the creation of  $V_o$  discussed above. In addition, the VB top of both samples was adjusted using five energy states or levels (see Figure 8b).

The level called  $\gamma$  at 10.3 eV in as-deposited  $TiO_2$  presents an increase of 0.65% after the HCHP process. This level may be related to the OH groups adsorbed on the surface of the films [44,52]. Furthermore, the  $\gamma$  level may also be related to Si impurity, which secretes from the substrate to the film [44,53]. Nevertheless, this latter possibility is unlikely, since the Si segregation was observed only in materials submitted to temperatures exceeding 800 °C [44]. Hannula et al. reported that this peak disappears after annealing at 400 °C in a vacuum or after 1 min of treatment at 300 °C under the  $H_2$  atmosphere [44]. In the present work, this contribution increases after plasma treatment, indicating that the energies involved in the process are not sufficient to eliminate OH groups from the surface of the films. Withal, the O2p nonbonding contribution, assigned to nonbonding O2p orbitals [44], tends to decrease ~6.5% after the HCHP process. This reinforces the XPS results discussed earlier that indicate the removal of O atoms from the film surface during the HCHP treatment. Based on this, it is possible to conclude that probably two phenomena are happening at the same time: (i) volatilization of O atoms and (ii) adsorption of OH species on the surface of the films. These phenomena can be explained by the chemical and physical reactions that occur during the HCHP treatment. When  $H^+$  ions bind to O on the film surface, the reaction product is volatile  $H_2O$  (see Equations (1), (2) and Figure 2a). As the water molecule is generated within the hollow cathode plasma, it can undergo dissociation, ionization and electron attachment processes, forming  $OH^-$  species that can be incorporated on the film surface.

The curves centered at 7.7 eV and 5.7 eV (for as-grown  $TiO_2$ ) are assigned to the  $\sigma$ - and  $\pi$ -type molecular orbitals of  $TiO_2$ , respectively [44]. The  $\sigma$ -type is mainly related to O2p<sub>z</sub>, while the  $\pi$ -type to O2p<sub>x</sub> and O2p<sub>y</sub> [54,55]. In Figure 8b, we can see that the concentration of  $\sigma$ -type orbitals in the pristine  $TiO_2$  is majority at the top of the VB, a common behavior in pure  $TiO_2$  [45]. After the HCHP treatment, the contribution of the  $\pi$ -type orbitals increased ~8.56%, while the  $\sigma$ -type decreased ~4.94%. It is observed that the TS is caused mainly by the increase of the  $\pi$ -type bond states.

The curve centered on 0.8 eV is commonly related to mid-gap states induced by dopants  $Ti^{3+/2+}$  interstitial or  $V_o$  [44]. In the pristine  $TiO_2$  film, the presence of these states contributes only to 0.6% of the states present at the top of the VB. The presence of this peak in the pristine  $TiO_2$  film agrees with the O1s states discussed in Figure 6 and may be related to the intrinsic defects of  $TiO_2$ . After the HCHP process, this contribution increased significantly to 2.9%. The position of this peak remains practically constant at 0.8 eV and is consistent with the theoretically obtained value to  $Ti^{3+}$  (0.8 eV),  $V_o$  (0.7 eV) and  $Ti^{3+}$ -OH (0.4 eV) [56], indicating the creation/increase of the  $Ti^{3+/2+}$  states. These states, along with the tail states, provide shorter-energy transitions to CB than the direct bandgap transitions, explaining the sub-gap absorption in visible and NIR (see Figure 6a).

As previously presented, the HCHP process of anatase  $TiO_2$  films results in a reduction of  $Ti^{4+}$ . An excess of electrons in the energy levels close to the CB is caused by the induced  $V_o$  due to the removal of oxygen of the  $TiO_2$  lattice [57], increasing its conductivity. In fact, by four-point probe analysis (see Table 1), we observed a significant decrease in resistivity after the hydrogenation process. Considering that the measuring range of the four-point probe equipment is 10 M $\Omega$ /sq, the resistivity reduction was at least 99.8%.

#### 2.4. Photocatalytic Activity

The photocatalytic activity (PA) of  $TiO_2$  thin films was evaluated by measuring the MB optical absorption by a UV-vis spectrophotometer. Prior to exposing the samples to the UV-visible light source, they were kept in the MB solution for 2 h to reach the adsorption/desorption stability. Then, the first absorbance measurement ( $C_0$ ) was performed. Finally, the light source was turned on and measurements were taken every 10 min.

Figure 9a,b presents the MB degradation ( $C_0/C$ ) as a function of UV-visible light irradiation time and the kinetic plot for pure MB solution, pristine  $\text{TiO}_2$  and black  $\text{TiO}_2$  films, respectively. In Figure 9b, a linear behavior can be observed for all samples. This behavior allowed us to use the equation below:

$$\ln \frac{C_0}{C} = kt, \quad (3)$$

where  $C$  is the concentration after a determined period of UV-visible light irradiation,  $t$  represents the irradiation time, and  $k$  the apparent rate constant ( $\text{min}^{-1}$ ) [58,59]. The constant  $k$  is known to be independent of the dye concentration or temperature, whereas photodegradation is a function that depends only on the irradiation flux and light source spectrum [59,60].

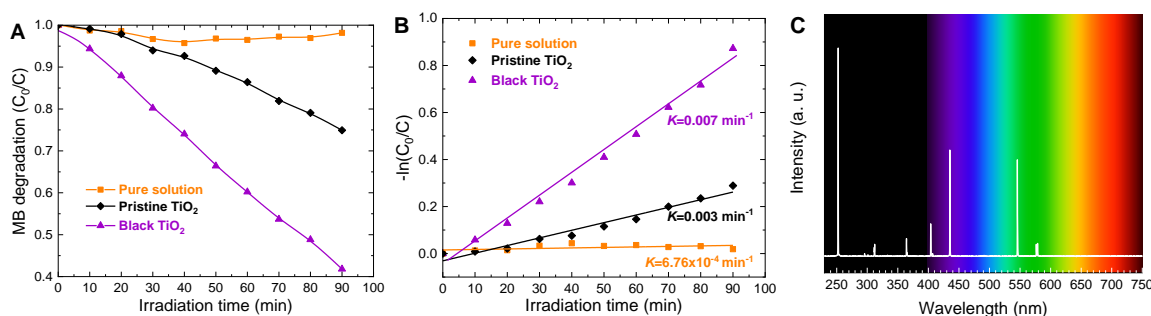


**Figure 9.** (A) UV-visible light driven photocatalytic decomposition of methylene blue (MB); (B) the kinetic with its respective apparent rate constant ( $k$ ) value for the pure solution (control), pristine, and black  $\text{TiO}_2$  thin films; and (C) the radiation emission spectrum of the UV-visible germicide lamp used in the photocatalytic assays.

First, it can be seen that the pure MB solution did not exhibit considerable photobleaching under exposure to UV-visible light, presenting a  $k$  value of  $6.76 \times 10^{-4} \text{ min}^{-1}$  (see Figure 9b). We can also point out that the black  $\text{TiO}_2$  thin film showed significant improvement in its PA compared to the pristine  $\text{TiO}_2$  film. Figure 9b shows that the black  $\text{TiO}_2$  sample has  $k = 7 \times 10^{-3} \text{ min}^{-1}$ , which is more than twice as great as the pristine sample, since the latter had a  $k$  value of  $3 \times 10^{-3} \text{ min}^{-1}$ . The apparent quantum efficiency of both films was estimated at 0.01% and 0.02% for pristine and black  $\text{TiO}_2$  samples, respectively. Compared to the results of Yan et al. [23], who reported the fastest hydrogen plasma treatment to blacken  $\text{TiO}_2$  nanomaterials, the best sample exposed to the  $\text{H}_2$  plasma showed an enhance of  $\sim 34\%$  in  $k$  against  $\sim 57\%$  of the present work. This can be explained by the fact that the hydrogenated sample of their work shows an increase of absorbance practically imperceptible in the visible range in comparison with the pristine  $\text{TiO}_2$ , while our black  $\text{TiO}_2$  thin film presented an increase of  $\sim 50\%$  in the absorbance in the visible and near IR range after HCHP treatment. It is important to highlight that our light source does not emit radiation in the NIR range (see Figure 9c). Hence, the improvement of the photocatalytic performance after HCHP treatment may be attributed to the combination of higher surface area ( $\sim 24\%$  increase compared to pristine  $\text{TiO}_2$ , Table 1), better electron mobility (reduced sheet resistance, Table 1), and absorption of the black  $\text{TiO}_2$  films (Figure 7a). As discussed in the previous sections, this light absorption improvement can be attributed to the changes induced by the increase of  $\text{Ti}^{3+/2+}$  and  $\text{V}_0$  in the film lattice, responsible for the improvement of the optical and electronic properties [48,57], i.e., increased light absorbance, due to the presence of defects states and TS within the bandgap. All of these changes may play an important role in the improvement of the degradation performance of the photocatalysts, what has to be better investigated in future works. In addition, the XPS results presented above revealed an increase in the amount of OH groups on the film surface after HCHP treatment. These OH species can react with holes in the valence band to generate OH radicals which have been reported to be the main oxidative group in photocatalysis reactions using  $\text{TiO}_2$  as photocatalysts, due to their main role in dissolution of organic molecules [39]. Therefore,

the greater presence of these groups on the black TiO<sub>2</sub> surface also contributed to the improvement of MB degradation. Finally, the ~24% increase of surface area obtained by the black TiO<sub>2</sub> film (see Section 2.1) also probably influenced the better PA performance after the HCHP process, since the surface area is an essential factor to improve degradation of the dye/contaminant [61].

### 3. Materials and Methods

#### 3.1. Substrate Cleaning and Preparation of TiO<sub>2</sub> Film

Pieces of 2 × 2 cm<sup>2</sup> of cover glass (Perfecta, ExaCta, São Paulo, Brazil) and 0.5 × 0.5 cm<sup>2</sup> of c-Si (100) (p-type, UniversityWafer Inc., South Boston, VA, USA) were used as substrates. Before the deposition process, the glass substrates were sonicated for 8 min with ethyl alcohol, acetone, and isopropyl alcohol. The c-Si substrates were cleaned by hydrogen peroxide + sulfuric acid solution (H<sub>2</sub>SO<sub>4</sub>/H<sub>2</sub>O<sub>2</sub>, 4:1) for 10 min, washed with deionized (DI) water and subjected to a solution of hydrofluoric acid with DI water (HF/H<sub>2</sub>O, 1:10) for 1 min and then rewashed with DI water.

The direct current (DC) magnetron sputtering (MS) technique was used for the pristine TiO<sub>2</sub> deposition. Details of the MS reactor can be found in reference [62]. The target used was a 34 mm diameter titanium plate (99.999%, Kurt J. Lesker, Jefferson Hills, PA, USA) and was set up 30 mm from the substrates. Sputtering was done using a gas mixture of argon (99.999%, White Martins, Jacareí, SP, Brazil) plus oxygen (99.999%, White Martins, Jacareí, SP, Brazil) at 15.0 sccm and 3.0 sccm of flow, respectively. The working pressure was fixed in 1.3 Pa and the residual pressure was 5.0 × 10<sup>-3</sup> Pa using a vacuum system composed of a diffusion plus mechanical pump system (Edwards, Burgess Hill, SXW, United Kingdom). The deposition process lasted 30 min and the plasma was sustained by 150 W of DC power (Advanced Energy, model MDX 1K, Fort Collins, CO, USA). No external heating was used during the deposition stage, being the final substrate temperature of approx. 100 °C. This temperature is due to the energy transfer by the impinging of the plasma species on the sample surface. Subsequently, the as-grown TiO<sub>2</sub> film was submitted to a heat treatment at 450 °C for 2 h using a furnace (INTI, FT-1200, São Carlos, SP, Brazil) at atmospheric pressure and ambient air.

#### 3.2. Preparation of Black TiO<sub>2</sub>: Hollow Cathode Hydrogen Plasma Process

The HCHP treatment was carried out in a capacitive plasma reactor [63]. A cylindrical hollow cathode made of titanium (99.99%) was connected to the 13.56 MHz RF power supply (ENI, model ACG-10B-01, Andover, MA, USA) and set up in 200 W of power. The process lasted 15 min and the bias voltage was maintained at 380 V. The hollow cathode has the following dimensions: diameter = 30 mm and length = 120 mm. For treatment, pure hydrogen gas (99.999%, White Martins, Jacareí, SP, Brazil) with 45 sccm of flow was used. The working and residual pressures were 13.3 Pa and 5.0 × 10<sup>-2</sup> Pa, respectively. The vacuum ambient was performed by a roots plus mechanical pumps (Edwards, EH500, Burgess Hill, SXW, United Kingdom). The pristine TiO<sub>2</sub> sample was placed inside and onto the hollow cathode electrode as outlined in Figure 2a. The hollow cathode wall temperature was measured by an optical pyrometer (Raytek Corporation, Raynger 3I, Santa Cruz, CA, USA), reaching a maximum value of 260 °C after 8 min and maintaining until the end of the treatment.

#### 3.3. Material Characterization

For material characterization, we used the cover glass for XRD, Raman spectroscopy, spectrophotometry and electrical analyses, while the silicon was used for profilometry, AFM and XPS analyses.

The film thickness was inferred by mechanical profilometry (KLA-Tencor, model P-7, Milpitas, CA, USA). The surface area and morphology were analyzed by AFM (Shimadzu, SPM 9500J3, Kyoto, Japan). The film surface area was obtained by a data processing software (Shimadzu, SPM-9500 Series Version 2.4, Kyoto, Japan). Microstructural properties were evaluated by XRD (PANalytical Empyrean diffractometer, Malvern, United Kingdom) using Cu K<sub>α</sub> (1.5406 Å for K<sub>α1</sub>) as the incident radiation

source. The scanning speed was  $3.2^\circ/\text{min}$  in the range of  $20\text{--}80^\circ$ . We used a step of  $0.013^\circ$  and a measurement time of 60 s/step. Vibrational characterization was carried out by Raman spectroscopy (Horiba, Evolution, Kyoto, Japan) in a spectral resolution lower than  $1\text{ cm}^{-1}$ . The excitation was induced by a 532 nm laser (power  $< 10\text{ mW}$ ). XPS measurements (Kratos Axis Ultra spectrometer, Kyoto, Japan) were performed to analyze the surface composition using an Al  $K\alpha$  ( $h\nu = 1486.69\text{ eV}$ ) excitation source operating at 120 W. The analyzes of the XPS spectra were performed by CasaXPS software (Casa Software Ltd.a, version 2.1.0.1, Japan) using the Shirley background [64].

The sheet resistivity was evaluated by a four-point probe meter (Jandel test unit, model RM3000, Leighton Buzzard, Beds, United Kingdom). The measurements were performed at ambient pressure using  $100\text{ }\mu\text{A}$  in three different points of the sample and the mean values were considered.

Optical characterizations were carried out by an UV-Vis-NIR spectrophotometer (Jasco, model V-570, Easton, PA, USA) equipped with 150 mm integrating sphere apparatus. The transmittance measurements were performed in the range of 190–2500 nm at normal incidence. The optical bandgap was inferred from the Tauc plot method [65].

### 3.4. Photocatalysis Assays

To test the photocatalytic properties of black  $\text{TiO}_2$ , a qualitative experiment was carried out using the films deposited on glass substrate by detecting the degradation rate of methylene blue-dye (MB) using a homemade reactor equipped with 6 UV-visible germicide lamps with 15 W (Osram, model HNS G13 - G15T8/OF, Munich, BY, Germany), air-cooled. The radiation emission spectrum of these lamps is shown in Figure 9c. The lamps were fixed at a distance of 70 mm from the samples, which have an active area of  $2 \times 2\text{ cm}^2$ , delivering an irradiance of  $2.2\text{ mW}\cdot\text{cm}^{-2}$  at the sample position which was measured using a calibration cell (Abet Tech, model 15151, Milford, KS, USA), as reported elsewhere [66,67]. It is important to note that the main emission peak of the lamp (250 nm) is not detected by this reference cell who operates between  $\sim 300\text{--}1100\text{ nm}$  and, therefore, the irradiance can be slightly higher than the value herein reported. Samples were placed in 6 mL of deionized water mixed with 10 mg/L of MB inside a beaker equipped with a water jacket system, which maintained the solution at room temperature. First, the solution was maintained during 1 h in the dark, and only after that were the lamps turned on. The MB degradation was inferred by the UV-vis spectrophotometer (ThermoFischer Scientific, model Evolution 220, Waltham, MA, USA) every 10 min. The solution was stirred constantly during all the process described above. Apparent quantum efficiency (AQE) was roughly estimated following the procedure reported before with some modifications [67]. We used a polychromatic light in this case (same used for photocatalytic experiments), i.e., no band pass filter was used. Therefore, the wavelength chosen for the AQE calculation was 250 nm, since it is the most intense peak of the lamp, as observed in Figure 9c.

## 4. Conclusions

The HCHP is presented as a fast and an effective technique for hydrogenating pristine  $\text{TiO}_2$  thin films. The HCHP process provided an expressive improvement in the morphological, microstructural, optical, and electronic characteristics. These improvements occurred due to the increase of  $V_o$ ,  $\text{Ti}^{3+/2+}$  species and OH groups in the microstructure of hydrogenated  $\text{TiO}_2$  film. These microstructural changes also induced the formation of midgap states within the bandgap. In addition, an increase of the TS size in the VB was also observed, which directly influenced the increase in light absorption not only in UV range, but also in the visible and NIR range. Also, a significant increase in surface area was observed after the HCHP treatment. All these modifications were responsible for improving the photocatalytic performance of the black  $\text{TiO}_2$  thin film, when applied in the photocatalysis process under UV-visible light. In sum, in addition to presenting as an efficient method, the HCHP can be considered suitable for synthesizing black  $\text{TiO}_2$  films with essential properties for liquid decomposition photocatalysis and even other photoinduced applications.

**Author Contributions:** Conceptualization, A.G.J., A.P., R.P.; methodology, A.G.J., A.P., M.G., R.P., G.P., A.d.S.S., M.M., A.N., H.W.; analysis, A.G.J., A.P., M.G., W.M., D.L., A.N., H.W.; investigation, A.G.J., A.P., M.G., R.P., D.L., G.P., A.d.S.S.; resources, G.P., M.M., A.d.S.S., D.L., R.P., M.F.; data curation, A.G.J., A.P.; writing—original draft preparation, A.G.J., A.P.; writing—review and editing, A.G.J., A.P., M.G., M.F., R.P., D.L., G.P., W.M., M.M., A.d.S.S., A.N., H.W.; supervision, A.P., A.d.S.S., R.P.; project administration, A.d.S.S.; funding acquisition, G.P., M.M., A.d.S.S., D.L., R.P., M.F. All authors have read and agreed to the published version of the manuscript.

**Funding:** This research was funded by Brazilian research foundation agencies CAPES (Grant number 2010-8/555.686), CNPq (2012-9/201050, 2012-8/470820, 2018-6/159754 and 2018-5/307199), and FAPESP (2015/06241-5 and 2018/01265-1). This study was also funded by the Coordenação de Aperfeiçoamento de Pessoal de Nível Superior—Brazil (CAPES)—Finance Code 001 and Capes-Print program, by the National Council for Scientific and Technological Development (CNPq; process numbers 486342/2013-1, 427835/2016-0, and 310066/2017-4), and by the Foundation for Support to the Development of Teaching, Science and Technology of the State of Mato Grosso do Sul (FUNDECT, process N° 23/200.247/2014). A.N. greatly appreciate the funding received from FUNDECT Ph.D. funding.

**Acknowledgments:** The authors thank the Associated Laboratory of Sensors and Materials, LABAS of the National Institute of Space Research, INPE for the XPS analysis, and Fábio Dondeo of the Institute for Advanced Studies (IEAv)—Photonics Division (EFO) for the UV-Vis measurements.

**Conflicts of Interest:** The authors declare no conflict of interest.

## References

1. Ikeda, S.; Fujikawa, S.; Harada, T.; Nguyen, T.H.; Nakanishi, S.; Takayama, T.; Iwase, A.; Kudo, A. Photocathode characteristics of a spray-deposited Cu<sub>2</sub>ZnGeS<sub>4</sub> thin film for CO<sub>2</sub> reduction in a CO<sub>2</sub>-saturated aqueous solution. *Appl. Energy Mater.* **2019**, *2*, 6911–6918. [[CrossRef](#)]
2. Nogueira, A.E.; Oliveira, J.A.; da Silva, G.T.; Ribeiro, C. Insights into the role of CuO in the CO<sub>2</sub> photoreduction process. *Sci. Rep.* **2019**, *9*, 1–11. [[CrossRef](#)] [[PubMed](#)]
3. Zhou, R.; Guzman, M.I. CO<sub>2</sub> reduction under periodic illumination of ZnS. *J. Phys. Chem. C* **2014**, *118*, 11649–11656. [[CrossRef](#)]
4. Fujishima, A.; Honda, K. Electrochemical photolysis of water at a semiconductor electrode. *Nature* **1972**, *238*, 37–38. [[CrossRef](#)]
5. Sun, C.; Jia, Y.; Yang, X.H.; Yang, H.G.; Yao, X.; Lu, G.Q.; Selloni, A.; Smith, S.C. Hydrogen incorporation and storage in well-defined nanocrystals of anatase titanium dioxide. *J. Phys. Chem. C* **2011**, *115*, 25590–25594. [[CrossRef](#)]
6. Chen, X.; Selloni, A. Introduction: Titanium dioxide (TiO<sub>2</sub>) nanomaterials. *Chem. Rev.* **2014**, *114*, 9281–9282. [[CrossRef](#)]
7. Duarte, D.A.; Massi, M.; Da Silva Sobrinho, A.S. Development of dye-sensitized solar cells with sputtered N-Doped TiO<sub>2</sub> thin films: From modeling the growth mechanism of the films to fabrication of the solar cells. *Int. J. Photoenergy* **2014**, *2014*, 1–13. [[CrossRef](#)]
8. Duarte, D.A.; Massi, M.; Sagás, J.C.; Da Silva Sobrinho, A.S.; Irala, D.R.; Fontana, L.C. Hysteresis-free deposition of TiO<sub>x</sub>N<sub>y</sub> thin films: Effect of the reactive gas mixture and oxidation of the TiN layers on process control. *Vacuum* **2014**, *101*, 200–204. [[CrossRef](#)]
9. Pessoa, R.S.; Fraga, M.A.; Santos, L.V.; Massi, M.; Maciel, H.S. Nanostructured thin films based on TiO<sub>2</sub> and/or SiC for use in photoelectrochemical cells: A review of the material characteristics, synthesis and recent applications. *Mater. Sci. Semicond. Process.* **2015**, *29*, 56–68. [[CrossRef](#)]
10. Zaleska, A. Doped-TiO<sub>2</sub>: A Review. *Recent Patents Eng.* **2008**, *2*, 157–164. [[CrossRef](#)]
11. Li, F.; Dong, B. Construction of novel Z-scheme Cu<sub>2</sub>O/graphene/α-Fe<sub>2</sub>O<sub>3</sub> nanotube arrays composite for enhanced photocatalytic activity. *Ceram. Int.* **2017**, *43*, 16007–16012. [[CrossRef](#)]
12. Aguirre, M.E.; Zhou, R.; Eugene, A.J.; Guzman, M.I.; Grela, M.A. Cu<sub>2</sub>O/TiO<sub>2</sub> heterostructures for CO<sub>2</sub> reduction through a direct Z-scheme: Protecting Cu<sub>2</sub>O from photocorrosion. *Appl. Catal. B Environ.* **2017**, *217*, 485–493. [[CrossRef](#)]
13. Chen, X.; Liu, L.; Yu, P.Y.; Mao, S.S. Increasing solar absorption for photocatalysis with black hydrogenated titanium dioxide nanocrystals. *Science* **2011**, *331*, 746–750. [[CrossRef](#)] [[PubMed](#)]
14. Naldoni, A.; Allieta, M.; Santangelo, S.; Marelli, M.; Fabbri, F.; Cappelli, S.; Bianchi, C.L.; Psaro, R.; Dal Santo, V. Effect of nature and location of defects on bandgap narrowing in black TiO<sub>2</sub> nanoparticles. *J. Am. Chem. Soc.* **2012**, *134*, 7600–7603. [[CrossRef](#)] [[PubMed](#)]

15. Wei, S.; Wu, R.; Jian, J.; Chen, F.; Sun, Y. Black and yellow anatase titania formed by (H,N)-doping: Strong visible-light absorption and enhanced visible-light photocatalysis. *Dalt. Trans.* **2015**, *44*, 1534–1538. [[CrossRef](#)] [[PubMed](#)]
16. Chen, X.; Zhao, D.; Liu, K.; Wang, C.; Liu, L.; Li, B.; Zhang, Z.; Shen, D. Laser-Modified Black Titanium Oxide Nanospheres and Their Photocatalytic Activities under Visible Light. *ACS Appl. Mater. Interfaces* **2015**, *7*, 16070–16077. [[CrossRef](#)] [[PubMed](#)]
17. Teng, F.; Li, M.; Gao, C.; Zhang, G.; Zhang, P.; Wang, Y.; Chen, L.; Xie, E. Preparation of black TiO<sub>2</sub> by hydrogen plasma assisted chemical vapor deposition and its photocatalytic activity. *Appl. Catal. B Environ.* **2014**, *148*, 339–343. [[CrossRef](#)]
18. Zhu, G.; Shan, Y.; Lin, T.; Zhao, W.; Xu, J.; Tian, Z.; Zhang, H.; Zheng, C.; Huang, F. Hydrogenated blue titania with high solar absorption and greatly improved photocatalysis. *Nanoscale* **2016**, *8*, 4705–4712. [[CrossRef](#)]
19. Kang, Q.; Cao, J.; Zhang, Y.; Liu, L.; Xu, H.; Ye, J. Reduced TiO<sub>2</sub> nanotube arrays for photoelectrochemical water splitting. *J. Mater. Chem. A* **2013**, *1*, 5766–5774. [[CrossRef](#)]
20. Wang, Z.; Yang, C.; Lin, T.; Yin, H.; Chen, P.; Wan, D.; Xu, F.; Huang, F.; Lin, J.; Xie, X.; et al. H-doped black titania with very high solar absorption and excellent photocatalysis enhanced by localized surface plasmon resonance. *Adv. Funct. Mater.* **2013**, *23*, 5444–5450. [[CrossRef](#)]
21. Wu, H.; Xu, C.; Xu, J.; Lu, L.; Fan, Z.; Chen, X.; Song, Y.; Li, D. Enhanced supercapacitance in anodic TiO<sub>2</sub> nanotube films by hydrogen plasma treatment. *Nanotechnology* **2013**, *24*, 455401. [[CrossRef](#)] [[PubMed](#)]
22. Yan, Y.; Hao, B.; Wang, D.; Chen, G.; Markweg, E.; Albrecht, A.; Schaaf, P. Understanding the fast lithium storage performance of hydrogenated TiO<sub>2</sub> nanoparticles. *J. Mater. Chem. A* **2013**, *1*, 14507–14513. [[CrossRef](#)]
23. Yan, Y.; Han, M.; Kokin, A.; Koppe, T.; Wang, D.; Andreu, T.; Chen, G.; Vetter, U.; Morante, J.R.; Schaaf, P. Slightly hydrogenated TiO<sub>2</sub> with enhanced photocatalytic performance. *J. Mater. Chem. A* **2014**, *2*, 12708–12716. [[CrossRef](#)]
24. Panomsuwan, G.; Watthanaphanit, A.; Ishizakiae, T.; Saito, N. Water-plasma-assisted synthesis of black titania spheres with efficient visible-light photocatalytic activity. *Phys. Chem. Chem. Phys.* **2015**, *17*, 13794–13799. [[CrossRef](#)]
25. Mohammadzadeh, M.R.; Bagheria, M.; Aghabagheria, S.; Abdiba, Y. Photocatalytic activity of TiO<sub>2</sub> thin films by hydrogen DC plasma. *Appl. Surf. Sci.* **2015**, *350*, 43–49. [[CrossRef](#)]
26. Islam, S.Z.; Reed, A.; Nagpure, S.; Wanninayake, N.; Browning, J.F.; Strzalka, J.; Kim, D.Y.; Rankin, E. Hydrogen incorporation by plasma treatment gives mesoporous black TiO<sub>2</sub> thin films with visible photoelectrochemical water oxidation activity. *Microporous Mesoporous Mater.* **2017**, *261*, 35–43. [[CrossRef](#)]
27. Carp, O.; Huisman, C.L.; Reller, A. Photoinduced reactivity of titanium dioxide. *Prog. Solid State Chem.* **2004**, *32*, 33–177. [[CrossRef](#)]
28. Ullattil, S.G.; Narendranath, S.B.; Pillai, S.C.; Periyat, P. Black TiO<sub>2</sub> Nanomaterials: A Review of Recent Advances. *Chem. Eng. J.* **2018**, *343*, 708–736. [[CrossRef](#)]
29. Li, L.; Chen, Y.; Jiao, S.; Fang, Z.; Liu, X.; Xu, Y.; Pang, G.; Feng, S. Synthesis, microstructure, and properties of black anatase and B phase TiO<sub>2</sub> nanoparticles. *Mater. Des.* **2016**, *100*, 235–240. [[CrossRef](#)]
30. Ge, M.; Cai, J.; Iocozzia, J.; Cao, C.; Huang, J.; Zhang, X.; Shen, J.; Wang, S.; Zhang, S.; Zhang, K.-Q.; et al. A review of TiO<sub>2</sub> nanostructured catalysts for sustainable H<sub>2</sub> generation. *Int. J. Hydrogen Energy* **2017**, *42*, 8418–8449. [[CrossRef](#)]
31. Zhu, G.; Xu, J.; Zhao, W.; Huang, F. Constructing black titania with unique nanocage structure for solar desalination. *ACS Appl. Mater. Interfaces* **2016**, *8*, 31716–31721. [[CrossRef](#)]
32. Ullattil, S.G.; Thelappurath, A.V.; Tadka, S.N.; Kavil, J.; Vijayan, B.K.; Periyat, P. A Sol-solvothermal Processed ‘Black TiO<sub>2</sub>’ as Photoanode Material in Dye Sensitized Solar Cells. *Sol. Energy* **2017**, *155*, 490–495. [[CrossRef](#)]
33. Zhi, J.; Yang, C.; Lin, T.; Cui, H.; Wang, Z.; Zhang, H.; Huang, F. Flexible all solid state supercapacitor with high energy density employing black titania nanoparticles as a conductive agent. *Nanoscale* **2016**, *8*, 4054–4062. [[CrossRef](#)] [[PubMed](#)]
34. Mou, J.; Lin, T.; Huang, F.; Chen, H.; Shi, J. Black titania-based theranostic nanoplatfor for single NIR laser induced dual-modal imaging-guided PTT/PDT. *Biomaterials* **2016**, *84*, 13–24. [[CrossRef](#)] [[PubMed](#)]
35. Muhl, S.; Pérez, A. The use of hollow cathodes in deposition processes: A critical review. *Thin Solid Film.* **2015**, *579*, 174–198. [[CrossRef](#)]

36. Pessoa, R.S.; Sagás, J.C.; Rodrigues, B.V.M.; Galvão, N.K.A.M.; Fraga, M.A.; Petracconi, G.; Maciel, H.S. Experimental studies on low-pressure plane-parallel hollow cathode discharges. *Braz. J. Phys.* **2018**, *48*, 411–420. [[CrossRef](#)]
37. Pessoa, R.S.; Sismanoglu, B.N.; Amorim, J.; Maciel, H.S.; Petracconi, G. *Gas Discharges: Fundamentals and Applications*; de Amorim Filho, J., Ed.; Transworld Research Network: Kerala, India, 2017; Volume 1, pp. 175–190.
38. Wang, F.H.; Chao, J.C.; Liu, H.W.; Liu, F.J. Physical properties of TiO<sub>2</sub>-doped zinc oxide thin films: Influence of plasma treatment in H<sub>2</sub> and/or Ar gas ambient. *Vacuum* **2017**, *140*, 155–160. [[CrossRef](#)]
39. Baik, S.J.; Jang, J.H.; Lee, C.H.; Cho, W.Y.; Lim, K.S. Highly textured and conductive undoped ZnO film using hydrogen post-treatment. *Appl. Phys. Lett.* **1997**, *70*, 3516–3518. [[CrossRef](#)]
40. Zhang, H.; Xing, Z.; Zhang, Y.; Li, Z.; Wu, X.; Liu, C.; Zhu, Q.; Zhou, W. Ni<sup>2+</sup> and Ti<sup>3+</sup> co-doped porous black anatase TiO<sub>2</sub> with unprecedented-high visible-light-driven photocatalytic degradation performance. *RSC Adv.* **2015**, *5*, 107150–107157. [[CrossRef](#)]
41. Tian, F.; Zhang, Y.; Zhang, J.; Pan, C. Raman spectroscopy: A new approach to measure the percentage of anatase TiO<sub>2</sub> exposed (001) facets. *J. Phys. Chem. C* **2012**, *116*, 7515–7519. [[CrossRef](#)]
42. Testoni, G.E.; Chiappim, W.; Pessoa, R.S.; Fraga, M.A.; Miyakawa, M.; Sakane, K.K.; Galvão, N.K.A.M.; Vieira, L.; Maciel, H.S. Influence of the Al<sub>2</sub>O<sub>3</sub> partial-monolayer number on the crystallization mechanism of TiO<sub>2</sub> in ALD TiO<sub>2</sub>/Al<sub>2</sub>O<sub>3</sub> nanolaminates and its impact on the material properties. *J. Phys. D Appl. Phys.* **2016**, *49*, 375301. [[CrossRef](#)]
43. Han, J.X.; Cheng, Y.L.; Tu, W.B.; Zhan, T.Y.; Cheng, Y.L. The black and white coatings on Ti-6Al-4V alloy or pure titanium by plasma electrolytic oxidation in concentrated silicate electrolyte. *Appl. Surf. Sci.* **2018**, *428*, 684–697. [[CrossRef](#)]
44. Hannula, M.; Ali-Löytty, H.; Lahtonen, K.; Sarlin, E.; Saari, J.; Valden, M. Improved Stability of Atomic Layer Deposited Amorphous TiO<sub>2</sub> Photoelectrode Coatings by Thermally Induced Oxygen Defects. *Chem. Mater.* **2018**, *30*, 1199–1208. [[CrossRef](#)] [[PubMed](#)]
45. Bharti, B.; Kumar, S.; Lee, H.N.; Kumar, R. Formation of oxygen vacancies and Ti<sup>3+</sup> state in TiO<sub>2</sub> thin film and enhanced optical properties by air plasma treatment. *Sci. Rep.* **2016**, *6*, 32355. [[CrossRef](#)] [[PubMed](#)]
46. Wang, G.; Wang, H.; Ling, Y.; Tang, Y.; Yang, X.; Fitzmorris, R.C.; Wang, C.; Zhang, J.Z.; Li, Y. Hydrogen-Treated TiO<sub>2</sub> Nanowire Arrays for Photoelectrochemical Water Splitting. *Nano Lett.* **2011**, *11*, 3026–3033. [[CrossRef](#)] [[PubMed](#)]
47. Zhu, Y.; Liu, D.; Meng, M. H<sub>2</sub> spillover enhanced hydrogenation capability of TiO<sub>2</sub> used for photocatalytic splitting of water: A traditional phenomenon for new applications. *Chem. Commun.* **2014**, *50*, 6049–6051. [[CrossRef](#)] [[PubMed](#)]
48. Su, T.; Yang, Y.; Na, Y.; Fan, R.; Li, L.; Wei, L.; Yang, B.; Cao, W. An insight into the role of oxygen vacancy in hydrogenated TiO<sub>2</sub> nanocrystals in the performance of dye-sensitized solar cells. *ACS Appl. Mater. Interfaces* **2015**, *7*, 3754–3763. [[CrossRef](#)]
49. Katal, R.; Salehi, M.; Davood, M.H.; Farahani, A.; Masudy-Panah, S.; Ong, S.L.; Hu, J. Preparation of a New Type of Black TiO<sub>2</sub> under a Vacuum Atmosphere for Sunlight Photocatalysis. *ACS Appl. Mater. Interfaces* **2018**, *10*, 35316–35326. [[CrossRef](#)]
50. Wang, L.; Wu, D.; Guo, Z.; Yan, J.; Hu, Y.; Chang, Z.; Yuan, Q.; Ming, H.; Wang, J. Ultra-thin TiO<sub>2</sub> sheets with rich surface disorders for enhanced photocatalytic performance under simulated sunlight. *J. Alloys Compd.* **2018**, *745*, 26–32. [[CrossRef](#)]
51. Mattox, D.M. Particle bombardment effects on thin-film deposition: A review. *J. Vac. Sci. Technol. A Vac. Surf. Film.* **1989**, *7*, 1105–1114. [[CrossRef](#)]
52. Sanjinés, R.; Tang, H.; Berger, H.; Gozzo, F.; Margaritondo, G.; Lévy, F. Electronic structure of anatase TiO<sub>2</sub> oxide. *J. Appl. Phys.* **1994**, *75*, 2945–2951. [[CrossRef](#)]
53. Pessoa, R.S.; Tezani, L.L.; Maciel, H.S.; Petracconi, G.; Massi, M. Study of SF<sub>6</sub> and SF<sub>6</sub>/O<sub>2</sub> plasmas in a hollow cathode reactive ion etching reactor using Langmuir probe and optical emission spectroscopy techniques. *Plasma Sources Sci. Technol.* **2010**, *19*, 025013. [[CrossRef](#)]
54. Fulton, C.C.; Lucovsky, G.; Nemanich, R.J. Electronic states at the interface of Ti–Si oxide on Si(100). *J. Vac. Sci. Technol. B Microelectron. Nanom. Struct.* **2002**, *20*, 1726–1732. [[CrossRef](#)]

55. Pereira, A.L.J.; Lisboa Filho, P.N.; Acua, J.; Brandt, I.S.; Pasa, A.A.; Zanatta, A.R.; Vilcarrromero, J.; Beltrán, A.; Dias da Silva, J.H. Enhancement of optical absorption by modulation of the oxygen flow of TiO<sub>2</sub> films deposited by reactive sputtering. *J. Appl. Phys.* **2012**, *111*, 113513. [CrossRef]
56. Greiner, M.T.; Lu, Z.H. Thin-film metal oxides in organic semiconductor devices: Their electronic structures, work functions and interfaces. *NPG Asia Mater.* **2013**, *5*, e55. [CrossRef]
57. Di Valentin, C.; Pacchioni, G.; Selloni, A. Reduced and n-type doped TiO<sub>2</sub>: Nature of Ti<sup>3+</sup> species. *J. Phys. Chem. C* **2009**, *113*, 20543–20552. [CrossRef]
58. Lepcha, A.; Maccato, C.; Mettenboerger, A.; Andreu, T.; Mayrhofer, L.; Walter, M.; Olthof, S.; Ruoko, T.-P.; Klein, A.; Moseler, M.; et al. Electrospun Black Titania Nanofibres: Influence of Hydrogen Plasma Induced Disorder on the Electronic Structure and Photoelectrochemical Performance. *J. Phys. Chem. C* **2015**, *119*, 18835–18842. [CrossRef]
59. Chen, Y.; Wu, Q.; Liu, L.; Wang, J.; Song, Y. The fabrication of self-floating Ti<sup>3+</sup>/N co-doped TiO<sub>2</sub>/diatomite granule catalyst with enhanced photocatalytic performance under visible light irradiation. *Appl. Surf. Sci.* **2019**, *467–468*, 514–525. [CrossRef]
60. Chen, Y.; Liu, K. Fabrication of magnetically recyclable Ce/N co-doped TiO<sub>2</sub>/NiFe<sub>2</sub>O<sub>4</sub>/diatomite ternary hybrid: Improved photocatalytic efficiency under visible light irradiation. *J. Alloys Compd.* **2017**, *697*, 161–173. [CrossRef]
61. Wang, G.; Zheng, J.; Bi, H.; Wang, S.; Wang, J.; Sun, J.; Guo, Y.; Wang, C. Ti<sup>3+</sup> self-doping in bulk of rutile TiO<sub>2</sub> for enhanced photocatalysis. *Scr. Mater.* **2019**, *162*, 28–32. [CrossRef]
62. Toku, H.; Pessoa, R.S.; Maciel, H.S.; Massi, M.; Mengui, U.A. The effect of oxygen concentration on the low temperature deposition of TiO<sub>2</sub> thin films. *Surf. Coat. Technol.* **2008**, *202*, 2126–2131. [CrossRef]
63. Pessoa, R.S.; Maciel, H.S.; Petraconi, G.; Massi, M.; da Silva Sobrinho, A.S. Effect of gas residence time on the morphology of silicon surface etched in SF<sub>6</sub> plasmas. *Appl. Surf. Sci.* **2008**, *255*, 749–751. [CrossRef]
64. CasaXPS: Processing Software for XPS, AES. *SIMS More*. 2019. Version 2.1.0.1. Available online: <http://www.casaxps.com/> (accessed on 1 March 2020).
65. Chiappim, W.; Testoni, G.E.; Moraes, R.S.; Pessoa, R.S.; Sagás, J.C.; Origo, F.D.; Vieira, L.; Maciel, H.S. Structural, morphological, and optical properties of TiO<sub>2</sub> thin films grown by atomic layer deposition on fluorine doped tin oxide conductive glass. *Vacuum* **2016**, *123*, 91–102. [CrossRef]
66. Nogueira, A.C.; Gomes, L.E.; Ferencz, J.A.; Rodrigues, J.E.; Gonçalves, R.V.; Wender, H. Improved Visible Light Photoactivity of CuBi<sub>2</sub>O<sub>4</sub>/CuO Heterojunctions for Photodegradation of Methylene Blue and Metronidazole. *J. Phys. Chem. C* **2019**, *123*, 25680–25690. [CrossRef]
67. Gomes, L.E.; da Silva, M.F.; Gonçalves, R.V.; Machado, G.; Alcantara, G.B.; Caires, A.R.; Wender, H. Synthesis and visible-light-driven photocatalytic activity of Ta<sup>4+</sup> self-doped gray Ta<sub>2</sub>O<sub>5</sub> nanoparticles. *J. Phys. Chem. C* **2018**, *122*, 6014–6025. [CrossRef]

